

RESEARCH

Open Access



Analysis and experimental validation of disulfidptosis related genes solute carrier family 3 member 2 (SLC3A2) in endometrial cancer

Bo Wang^{1†}, Wantong Wang^{1†}, Yuting Wang^{1†}, Xin Wen¹, Zihao Wang¹, Hongrui Leng¹, Fanfei Kong^{1*†} and Xiaoxin Ma^{1*†}

Abstract

Disulfidptosis, a novel cell death paradigm triggered by disulfide stress, remains underexplored, particularly its implications for endometrial cancer (EC). This study focused on the prognostic significance of disulfidptosis-related genes (DRGs) in EC, highlighting the pivotal role of SLC3A2. To predict EC patient outcomes, we developed a model centered on DRGs, employing LASSO-Cox regression for its construction. The model revealed a strong correlation between DRG risk score, gene set enrichment analysis (GSEA), single-sample GSEA (ssGSEA), clinical characteristics, the tumor microenvironment (TME), and the response to immunotherapy. Key genes were pinpointed using random forest maps. To establish SLC3A2's oncogenic effects in EC, we conducted comprehensive studies including apoptosis, cell cycle, TRANSWELL, CCK-8, and tumor xenograft assays. SLC3A2 expression was further confirmed via qRT-PCR. The impact of SLC3A2 on EC's malignant behavior was corroborated through both in vitro and in vivo experiments.

Keywords Endometrial carcinoma (EC), Disulfidptosis-related genes (DRGs), Prognostic model, Tumor microenvironment (TME), Carrier family 3 member 2 (SLC3A2)

Introduction

Endometrial cancer (EC) ranks as the most common gynecologic malignancy in the United States, Europe, and various developed areas. Although early detection is frequent, leading to improved survival rates through

effective treatment, advanced EC stages typically have a poor prognosis [1, 2]. Consequently, discovering a novel molecular biomarker for precise EC diagnosis, treatment, and prognostic assessment is of paramount importance.

Disulfide can maintain the spatial structure of proteins, giving them physical and chemical stability through cross-linking between and within subunits [3, 4]. Disulfidptosis is a newly discovered way of cell death that differs from the previously discovered methods of apoptosis, ferroptosis and cuproptosis [5, 6]. Recent studies have shown that disulfidptosis plays an important role in tumor metabolism as Regulated cell death [7]. The earliest identified disulfide death gene, SLC7A11, when combined with glucose starvation, can consume intracellular NADPH, resulting in a large accumulation of intracellular disulfide molecules and rapid cell death [6]. Recent

[†]Bo Wang, Wantong Wang, and Yuting Wang have contributed equally to this work and co-first authors.

[†]Fanfei Kong and Xiaoxin Ma have contributed equally to this work.

*Correspondence:

Fanfei Kong

kong_laoler@126.com

Xiaoxin Ma

maxiaoxin666@aliyun.com

¹ Department of Obstetrics and Gynecology, Shengjing Hospital of China Medical University, No 39 Huaxiang Road, Tiexi District, Shenyang 110000, Liaoning, People's Republic of China



studies have shown that disulfidptosis related genes (DRGs) SLC7A11 play an important role in bone metabolic diseases [8]. Disulfidptosis has been shown to play an important role in a number of tumors, including liver cancer, lung cancer, and bladder cancers [9–11]. However, the role of DRGs in EC has not been reported. But the prognostic significance of DRGs in EC, and their relationship to immunotherapy and chemotherapy therapy, has remained largely elusive.

In our research, we undertook an extensive evaluation of genes prognostic for disulfidptosis. Utilizing LASSO regression, we developed a predictive model which established itself as an independent factor for forecasting EC outcomes. Through random forest analysis, we pinpointed solute carrier family 3 member 2 (SLC3A2) as a critical gene. To corroborate SLC3A2's significance in EC, we executed both in vivo and in vitro studies, offering fresh perspectives on EC prognosis and the realm of precision medicine.

Materials and methods

Data acquisition

We sourced clinical information and RNA sequencing data (FPKM format) from the TCGA database, with a specific focus on uterine corpus endometrial cancer (UCEC). This dataset encompassed RNA sequencing from 552 UCEC cases and 35 normal tissue samples, accompanied by clinical data for 541 patients. We identified 24 disulfidptosis-related genes (DRGs) as listed in Table S1, referenced from prior research [5, 12–15].

Identification of DRGs and construction of model

Our study involved a univariate Cox regression analysis of 24 disulfidptosis-related genes (DRGs). We utilized the "Limma" package to pinpoint differentially expressed DRGs. The TCGA dataset, our primary source for prognostic data on endometrial cancer (EC) patients, constrained our model's internal validation. We divided the TCGA-UCEC patient data into a training set ($n=272$) and a test set ($n=269$) for our analyses. In the training set, LASSO-penalized Cox regression was employed to refine our model [16]. We calculated the risk score by summing the expression levels of each gene, weighted by its corresponding coefficient. This led to the categorization of UCEC patients in the training group into high-risk or low-risk groups, based on a predefined cutoff. The model's efficacy was then evaluated using the test group. Further, we developed a nomogram incorporating clinical data of EC patients, comparing its predictive accuracy against existing models. For pathway enrichment analysis, Gene Set Enrichment Analysis (GSEA) was applied. We also explored the relationship between risk scores and immune functions in patients, using single-sample

GSEA (ssGSEA) analysis [17]. Key genes in our model were identified using R packages "randomForest" for random forest map analyses.

Tumor microenvironment analysis

We used the "ESTIMATE" R package to calculate immune and stromal scores for each sample in our study. Following this, we applied the "limma" package to examine the relationship between the calculated risk scores and both immune and stromal scores. To evaluate cancer stem cell (CSC) levels in each patient's tumor, we obtained epigenome and transcriptome data [18]. Using these datasets, we conducted correlation analyses to explore the association between risk scores and the presence of CSCs.

Human tissue specimens

Between 2019 and 2021, we collected 28 normal endometrial and 28 EC tissue samples from Shengjing Hospital of China Medical University. Prior to participation, all subjects provided informed consent, ensuring adherence to ethical standards. We gathered clinicopathological data for each participant. Histopathologically, all EC cases were confirmed as endometrial adenocarcinoma. Two experienced pathologists, following the International Federation of Gynecology and Obstetrics (FIGO 2009) guidelines, independently verified the EC diagnoses. It's important to note that none of the patients had undergone hormone therapy, radiotherapy, chemotherapy, or any other treatment before their surgery.

qRT-PCR

For RNA extraction from the samples, we employed the TRIzol reagent (Vazyme, Nanjing, China) adhering strictly to the manufacturer's guidelines. We then synthesized complementary DNAs (cDNAs) using Prime Script RT-polymerase, also from Vazyme. To quantify the expression of target genes, we used SYBR Green Premix (Vazyme) in combination with specific polymerase chain reaction (PCR) primers (Sangon Biotech, Shanghai, China). The details of these primer sequences are listed in Supplementary Table S2. We calculated fold changes in gene expression using the $2^{-\Delta\Delta CT}$ method.

Transfection of cells

We acquired shRNA sequences targeting SLC3A2 lentiviral vectors (JST scientific, Wuhan, China). Additionally, we sourced the overexpression plasmid of SLC3A2 (JST scientific, Wuhan, China). The specific shRNA sequences are detailed in Supplementary Table S3. To transfect cells with these shRNAs, we used Lipofectamine 3000, a product of Invitrogen, following the manufacturer's prescribed protocol.

Cell culture

Ishikawa and HEC-1A cells were cultured in distinct environments: ISHIKAWA cells in 1640 medium and HEC-1A cells in 5A medium, both sourced from Gibco in Carlsbad, CA, USA. These media were each enriched with 10% fetal bovine serum (FBS) and 1% penicillin–streptomycin, also supplied by Gibco. The cells were incubated in a humidified setting at 37 °C, within an atmosphere comprising 5% carbon dioxide (CO₂).

CCK-8 assay

HEC-1A and Ishikawa cells were cultured in 96-well plates. After seeding, we added 10 µL of CCK-8 reagent (Dojindo, Japan) to each well. The plates were then incubated at 37 °C in an atmosphere containing 5% CO₂ for 3 h. To measure the optical density at 450 nm (OD₄₅₀), we used a microplate reader. This measurement was conducted at four different time points: immediately after treatment (0 h), and then at 24, 48, and 72 h post-treatment.

Cell invasion assay

To evaluate cell invasion capabilities, our experiment utilized the TRANSWELL assay. We prepared TRANSWELL chambers with a pore size of 8 µm, coating them with a Matrigel solution to simulate the extracellular matrix. For conducting the assay, we introduced 200 µL of serum-free medium, containing 2×10^4 cells, into the upper chamber. Concurrently, 500 µL of medium enriched with 10% FBS was added to the lower chamber. The cells were fixed using 4% paraformaldehyde and subsequently stained with crystal violet after 24 h. This staining technique facilitated the visualization of cells that had successfully traversed through the Matrigel and adhered to the underside of the chamber. The migrated cells were imaged using a fluorescent inverted microscope (NIKON, Japan) at 200× magnification, and these images were subsequently analyzed for quantitative assessment.

Apoptosis assay

Following transfection, we processed 1×10^6 cells from each experimental group with a thorough wash in phosphate-buffered saline (PBS). Subsequently, these cells were incubated at room temperature in a dark environment with phycoerythrin (PE) and fluorescein isothiocyanate (FITC) dyes for a duration of 15 min. This step was crucial for labeling the cells for subsequent analysis. To determine the percentage of apoptotic cells in the different experimental groups, we performed flow cytometry analysis. This quantification was carried out using a

DxFLEX flow cytometer, provided by Beckman, located in Suzhou, China.

Cell cycle analysis

Following cell transfection, we harvested 1×10^6 cells and fixed them in 70% ethanol, storing the suspension at 4 °C overnight. After a subsequent rinse with phosphate-buffered saline (PBS), we added 100 µL of RNase A to the cell suspension and incubated it in a water bath at 37 °C for 30 min. Next, 400 µL of propidium iodide (PI) was introduced, followed by a further 30-min incubation at 4 °C in the dark. The resulting cell suspension was then analyzed using flow cytometry. This analysis enabled the assessment of cell distribution across different phases of the cell cycle.

Tumor xenografts in nude mice

BALB/cA-nu mice, aged between 4 and 6 weeks, were acquired from HFK Bioscience in Beijing, China. For the experiment, each mouse received a subcutaneous injection of 1×10^6 transfected cells in the axillary region. All animal experiments were meticulously conducted in compliance with the guidelines approved by the Scientific Research and New Technology Ethical Committee of Shengjing Hospital, affiliated with China Medical University. The growth of the grafts was monitored and quantified using a specific formula: tumor volumes (mm³) = length × (width²)/2. Tumor sizes were methodically measured every 4 days over a span of 28 days. At the conclusion of this period, the mice were humanely euthanized. The extracted tumors were then processed for histological examination: fixed in a 4% polysound solution, dehydrated, embedded in paraffin, and sectioned for immunohistochemical analysis. This meticulous process enabled detailed study of the tumors' characteristics and responses to the treatment.

Results

In our study, we constructed a model of disulfidptosis related genes that outperformed existing prognostic models. disulfidptosis related genes have not been studied in EC. Our study lays a foundation for future studies of disulfidptosis related genes in EC. In our constructed model, we screened out the key gene SLC3A2 and conducted in vitro and in vivo experiments. We demonstrate that SCL3A2 is a promising target for EC therapy (Fig. 1).

Construction of a prognostic model

Univariate Cox regression showed that 7 out of DRGs were correlated with overall survival (OS) (Fig. 2A). We then performed Lasso-Cox regression analysis on these OS-related DRGs and obtained our prognostic model according to the final result (Fig. 2B, C). Risk

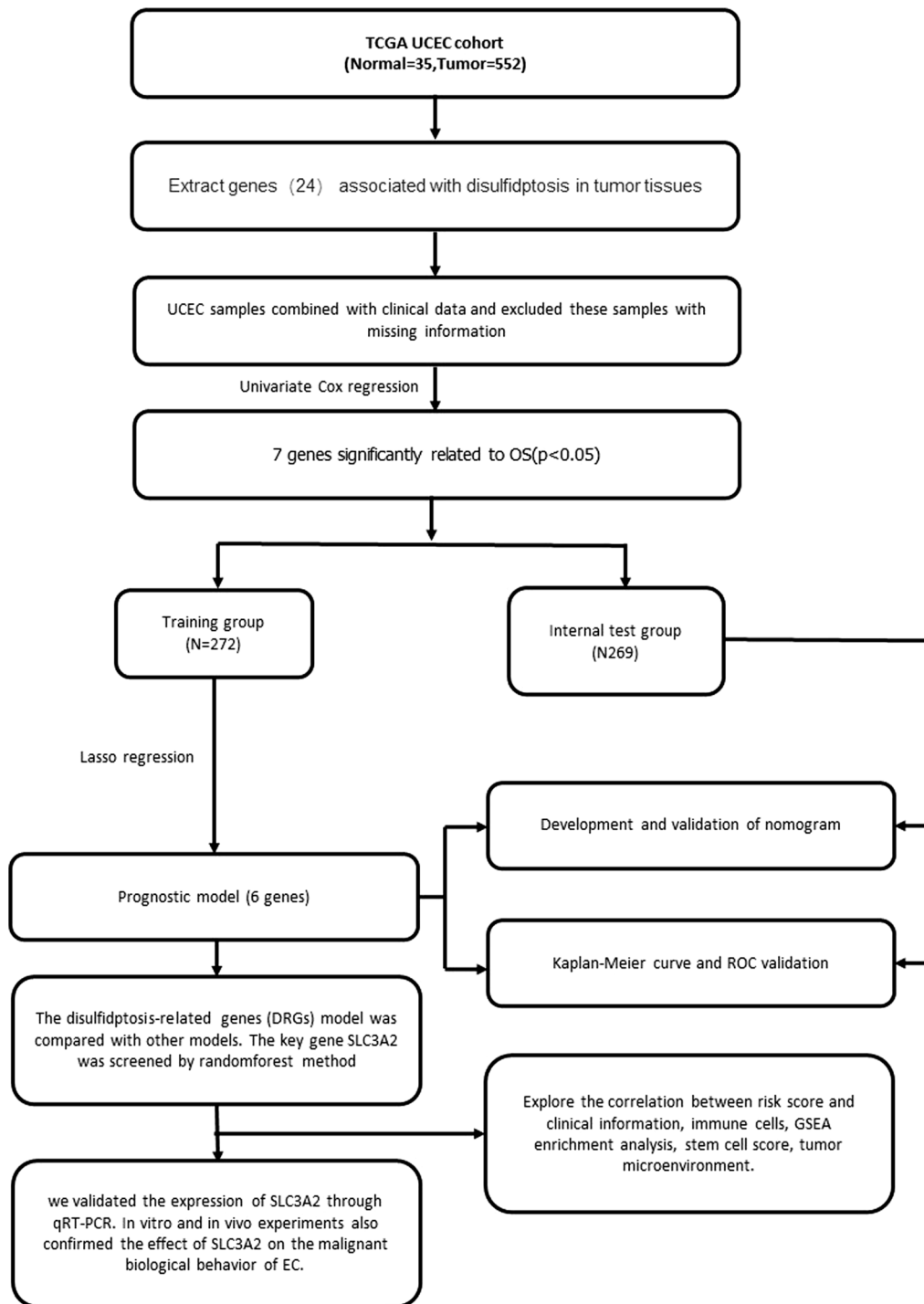


Fig. 1 Comprehensive prognostic value analysis framework of disulfidptosis-related genes (DRGs) in uterine corpus endometrial carcinoma (UCEC) patients based on TCGA database

score = $e^{((0.003 \times \text{Exp} [\text{ACTN4}] + (0.424 \times \text{Exp} [\text{INF2}] + (-0.107 \times \text{Exp} [\text{PDLIM1}] + (0.252 \times \text{Exp} [\text{SLC3A2}] + (0.454 \times \text{Exp} [\text{LRPPRC}] + (-0.613 \times \text{Exp} [\text{OXSM}])))$). The Kaplan–Meier (KM) analysis results showed that the high-risk group had a worse prognosis in

the training set compared to the low-risk group (Figure S1A). The area under the receiver operating characteristic (ROC) curves (AUCs) for 1-, 3-, and 5-year OS was calculated as 0.704, 0.751, and 0.727, respectively, in the

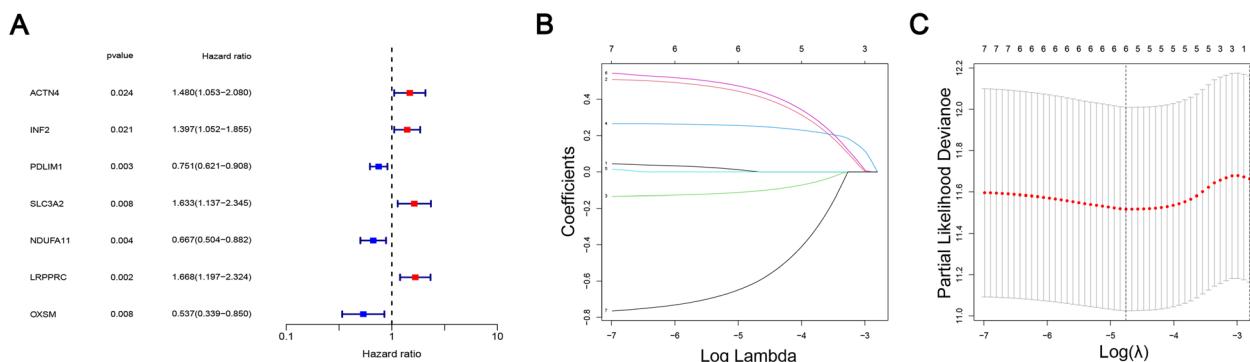


Fig. 2 Screening of prognosis DRGs and construction of prognosis model. **A** Univariate Cox regression analysis to identify the candidate prognosis-related hub DRGs in UCEC. **B** Partial likelihood deviation was plotted relative to the logarithm of lambda in tenfold cross-validation. **C** The trajectory graph of each variable

training group (Figure S1B). The distribution of patients' risk scores and survival status showed that the high-risk group did indeed have worse survival (Figure S1C-D). We ran the same tests on the model in the test set, and the results also showed that the high-risk group had worse survival (Figure S1E-H). This consistency across both training and test sets underscores the robustness and potential clinical relevance of this model.

Establishment of the nomogram

To enhance the predictive accuracy of our model, we devised a nomogram that integrates patients' clinical data (Fig. 3A). Calibration curves, presented in Fig. 3B, affirm the nomogram's commendable predictive performance. Additionally, both univariate and multivariate analyses, depicted in Figures S1I-1 J, established the risk score as an independent risk factor. The nomogram's effectiveness in predicting 1-, 3-, and 5-year OS rates was quantified, with the AUCs determined to be 0.795, 0.783, and 0.806,

respectively (Figure S1K). Decision curve analysis (DCA) further substantiated the nomogram's utility in clinical decision-making (Figure S1L). Comparative analysis using the ROC curve and KM plots (Fig. 4A, B) demonstrated that the DRG model possesses robust prognostic capabilities. When benchmarked against existing models [19–21], the concordance index (C-index) results highlighted in Fig. 4C indicate that our DRG model surpasses the predictive performance of these existing models. This underscores the DRG model's potential superiority in forecasting outcomes for endometrial cancer patients.

Association analysis of risk score

We further mined the model to analyze the correlation between the model and clinicopathological parameters, immune types, CSCs, and immune scores. Correlation analysis results showed that patients with higher levels of clinicopathological parameters (> 65 years, tumor grade 3–4, tumor stage III–IV) had higher risk scores

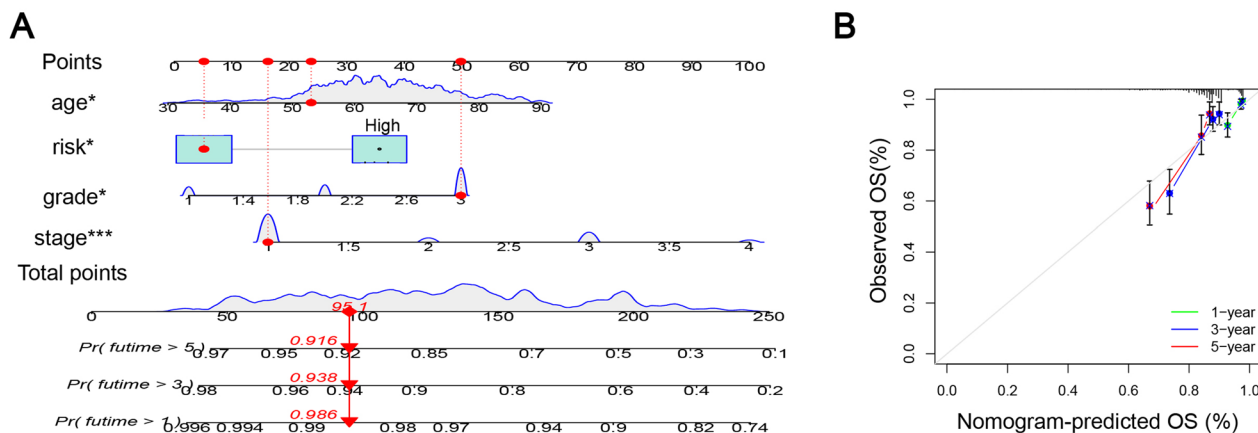


Fig. 3 Establishment of Nomogram. **A** Nomogram for predicting the 1-, 3-, and 5-year OS of UCEC patients. **B** Calibration curves for the prediction of 1-, 3- or 5-year overall survival of UCEC patients

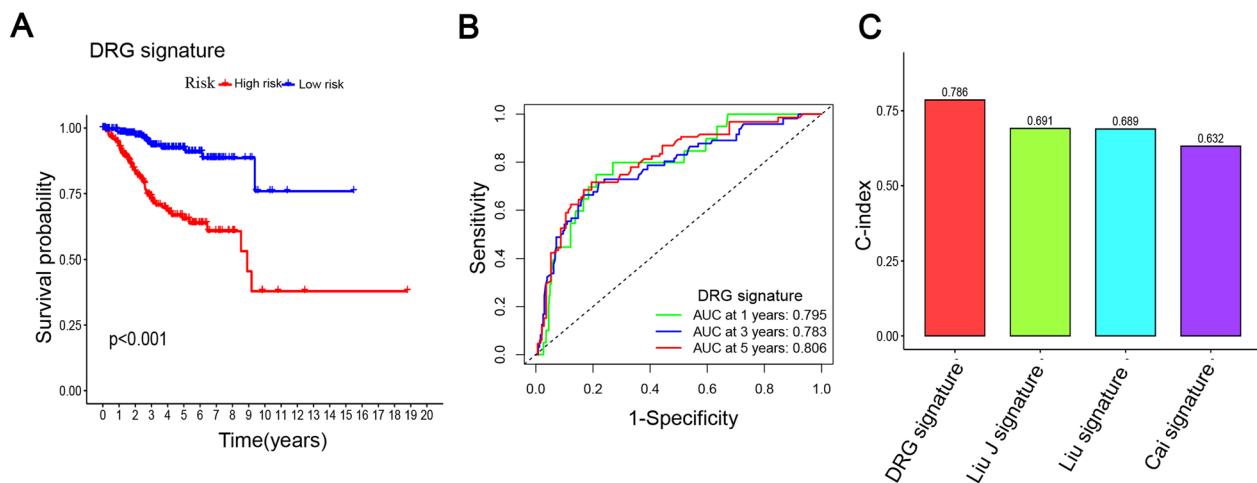


Fig. 4 Establishment of Nomogram and comparison with existing models. **A, B** Survival curves and ROC curves of high and low risk groups in the model constructed by us. **C** C-index comparison of DRG models with other models

(Fig. 5A–C). Moreover, our analysis exploring the links between immune subtypes and risk scores revealed a noteworthy finding: patients classified under the C2 immune subtype generally exhibited higher risk scores. This observation, depicted in Fig. 5D, correlates with a poorer prognosis for those within the C2 category.

SsGSEA provided insightful observations regarding the immune landscape in the context of risk groups. This analysis demonstrated that in the high-risk group, there was a general suppression of most immune cells and immune functions. Notably, the fractions of immune dendritic cells (iDCs), neutrophils, T helper cells, and tumor-infiltrating lymphocytes (TIL) were significantly reduced, as shown in Fig. 5E. Additionally, our analysis revealed that both checkpoint proteins and human leukocyte antigen (HLA) expressions were lower in the high-risk group, as illustrated in Fig. 5F. These findings are indicative of a compromised immune response in high-risk patients, which could be a factor contributing to their poorer prognosis. This underscores the importance of the immune system's role in cancer progression and the potential for targeted therapies that might enhance immune response in these patients.

We employed DNA stemness score (DNAss) and RNA stemness score (RNAss) as metrics to evaluate the levels of CSCs. Through correlation analysis, we discovered a positive correlation between the risk score and the RNAss, as depicted in Fig. 5G. This suggests that higher risk scores are associated with increased stemness characteristics at the RNA level in tumors. Conversely, the same correlation analysis revealed that the relationship between risk scores and the tumor microenvironment (TME), specifically in terms of immune and stromal scores, was not significant. This is also illustrated in

Fig. 5G. This finding indicates that while stemness characteristics are positively associated with risk scores, the overall influence of the TME, as measured by immune and stromal scores, does not show a significant correlation with the risk scores in our analysis.

The GSEA conducted in our study yielded significant findings regarding pathway activations in different risk groups. Notably, in the high-risk group, we observed substantial enrichments in a variety of biological pathways. These included chromosome segregation, cornification, keratinization, organelle fission, axon guidance, cell adhesion molecules, the cell cycle, and DNA replication. These enriched pathways are detailed in Fig. 5H, I. The identification of these significantly enriched pathways in the high-risk group provides a deeper understanding of the molecular mechanisms underpinning the aggressive nature of tumors in these patients. Such insights could be pivotal for developing targeted therapies and improving prognostic assessments in endometrial cancer.

Predicting the effects of immunotherapy sensitivity and anti-cancer treatment

The IMvigor210 database was downloaded to explore whether risk scores were associated with immunotherapy. Correlation analysis showed no significant difference in risk scores between patients with progressive disease (PD) or stable disease (SD) and patients with partial response (PR) or complete response (CR) (Fig. 6A). We further investigated the sensitivity of different risk groups to various chemotherapeutic agents. The results, as depicted in Fig. 6B–E, demonstrated a notable observation: patients in the high-risk group exhibited greater sensitivity to a range of chemotherapeutic drugs compared to those in the low-risk group. Specifically, the

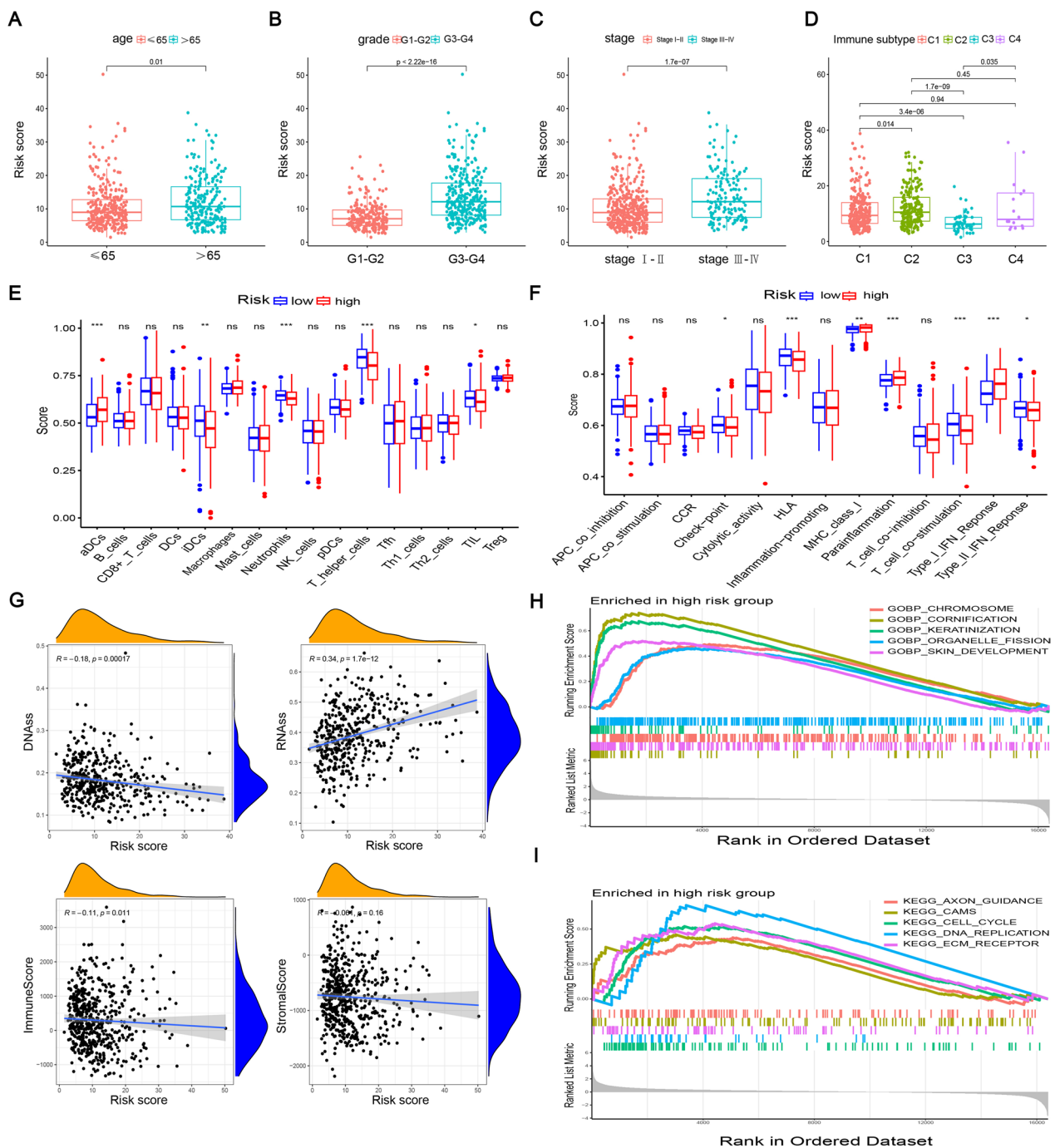


Fig. 5 Gene set enrichment analysis (GSEA) of biological functions and the association between risk score and tumor microenvironment. The risk score in different groups divided by age (A), grade (B), stage (C) and immune subtype (D). Comparison of the risk score in different immune infiltration. E, F The relationship between risk score and the scores of 16 immune cells and 13 immune-related functions were showed in boxplots. G The relationship between risk score and DNAss, RNAss, Stromal Score and Immune Score. H, I GSEA showed eleven pathways enriched in the high-risk group. P values were showed as: ns, not significant; *P < 0.05; **P < 0.01; ***P < 0.001

high-risk group showed increased responsiveness to cisplatin, dasatinib, doxorubicin, and paclitaxel. This finding suggests that despite the poorer prognosis associated

with the high-risk group, these patients may benefit more from treatment with these particular chemotherapeutic agents. Such insights are crucial for guiding treatment

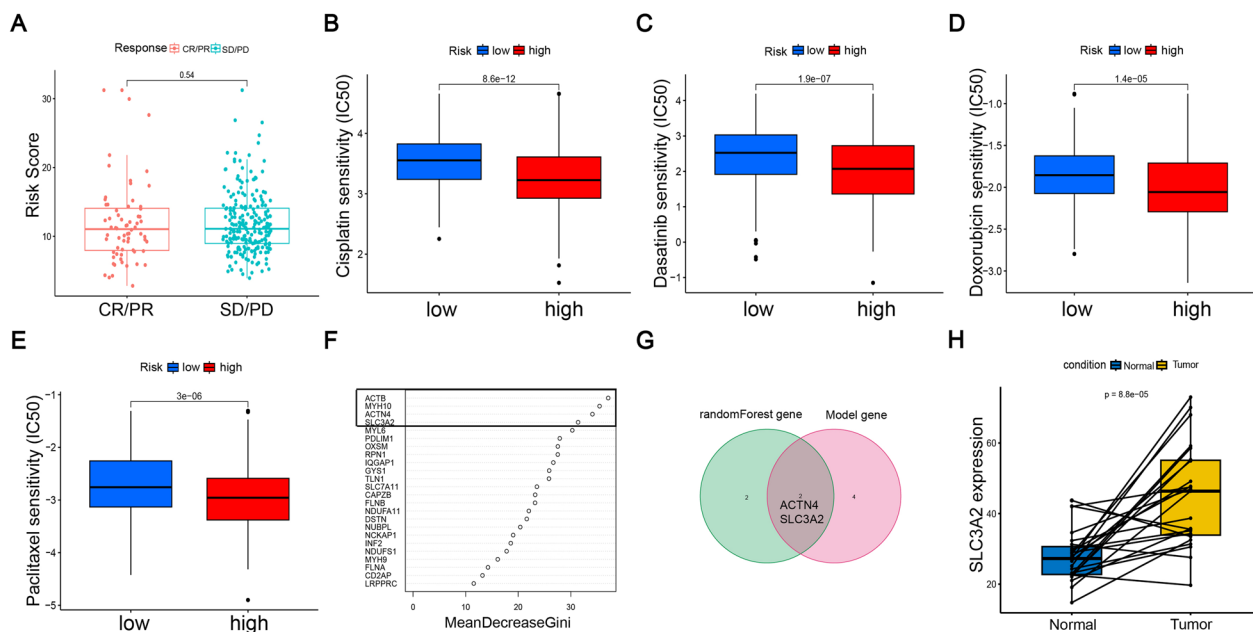


Fig. 6 Risk scores are associated with immunotherapy and chemotherapeutic drug response and Identification of key genes. **A** The correlation between risk scores and immunotherapy response. **B–E** The correlation between risk scores and chemotherapeutic drug sensitivity. **F** RandomForest error rate versus the number of classification trees. **G** The intersection genes of model gene and RandomForest were screened by Venn diagram. **H** Box plots showed the expression of SLC3A2 in normal and UCEC tissues from TCGA

decisions and tailoring therapy to individual patient profiles in the context of endometrial cancer.

Screening of key genes in the model

The results of random forest analysis showed the EC-related genes in 24 DRGs genes (Fig. 6F). We selected the top four genes in the random forest map as potential target genes (ACTB, MYH10, ACTN4, and SLC3A2). We intersected the four genes from the random forest with the genes from the model to get two key genes (ACTN4 and SLC3A2) (Fig. 6G). Considering that the coefficient of ACTN4 in the model formula is 0.003, on the other hand, univariate analysis shows that ACTN4 is a risk factor for EC after rain, but ACTN4 is low in EC, which has a certain contradiction. So we chose SLC3A2 as the target. We observed downregulation of SLC3A2 expression in the TCGA-UCEC dataset (Fig. 6H).

Experimental validation of SLC3A2

The results of qRT-PCR showed that SLC3A2 was significantly increased in EC (Fig. 7A). qRT-PCR results related to pathological parameters showed that SLC3A2 was upregulated in the EC of higher pathological parameters (>65 age group, tumor stage III–IV group, and lymph node (LN) metastasis group) (Fig. 7B–D).

The CCK8 assay was employed to evaluate the impact of SLC3A2 on the proliferation of EC cells. The CCK8

assay results for both ISHIKAWA and HEC-1A cell lines indicated that overexpression of SLC3A2 led to an enhancement in cell proliferation, whereas its knock-down resulted in a reduction of this process (Fig. 7E, F). Additionally, we observed that SLC3A2 overexpression spurred cell invasion, and conversely, SLC3A2 knock-down hindered invasion in these cell lines (Fig. 7G). The results from apoptosis experiments revealed that SLC3A2 overexpression was associated with decreased apoptosis, while knockdown of SLC3A2 facilitated increased apoptosis in both ISHIKAWA and HEC-1A cells (Fig. 8A). In terms of cell cycle dynamics, overexpression of SLC3A2 led to a higher proportion of cells in the G2-M phase, whereas its knockdown reduced the percentage of cells in this phase (Fig. 8B). In vivo experiments further substantiated these findings. The growth of tumors in the SLC3A2(-) group was significantly impeded compared to the SLC3A2(-)-NC group (Fig. 8C). Moreover, immunohistochemical analysis of KI-67, a marker for cell proliferation, on the transplanted tumors showed that SLC3A2 knockdown significantly reduced proliferation (Fig. 8D). These comprehensive results underscore the pivotal role of SLC3A2 in the proliferation, invasion, and survival of EC cells, thereby highlighting its potential as a target for therapeutic intervention in EC.

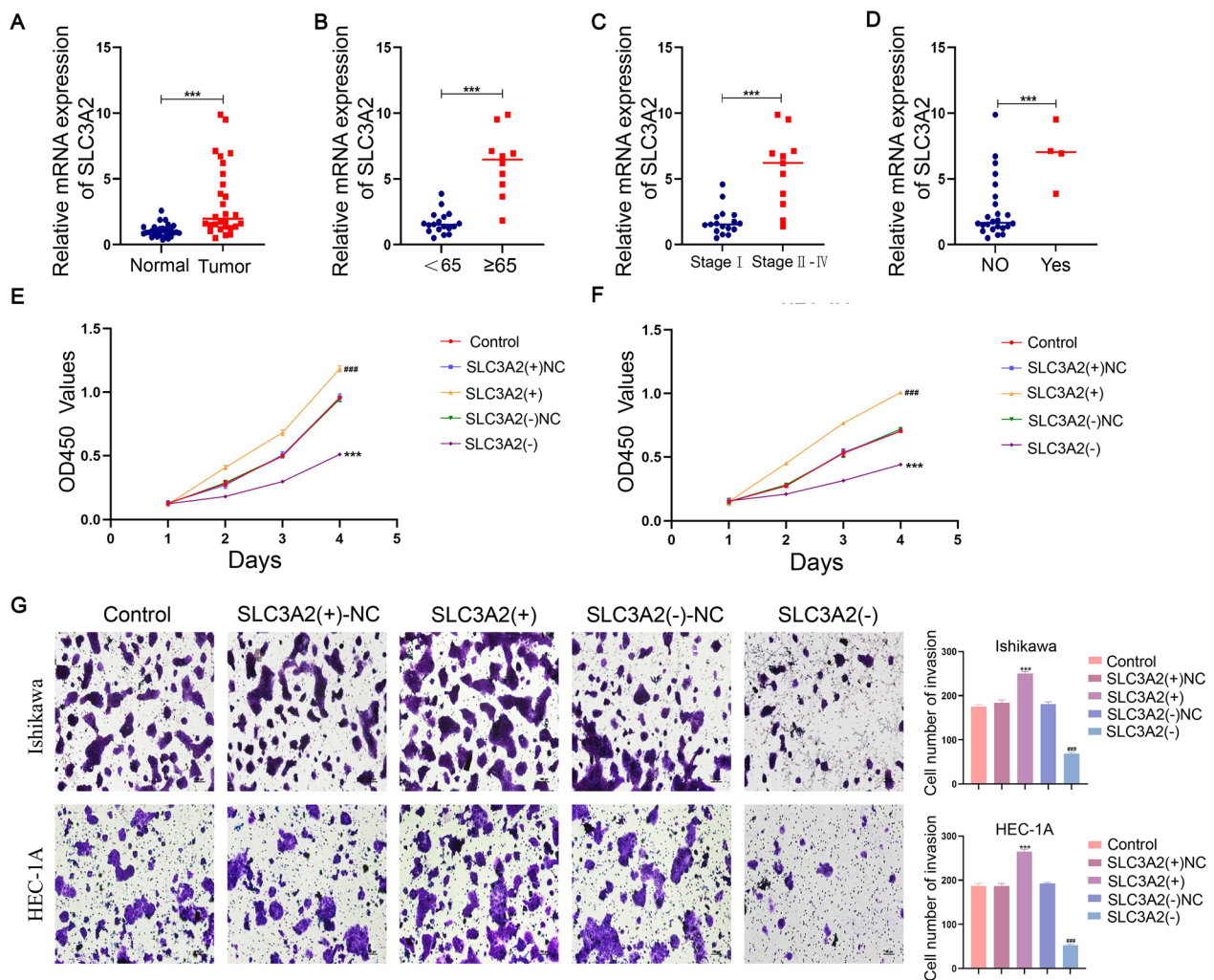


Fig. 7 SLC3A2 regulates the biological behavior of EC cell lines. **A** The results of qRT-PCR showed the expression of SLC3A2 in normal endometrial tissue (n = 28) and human endometrial carcinoma tissue (n = 28). The expression of SLC3A2 in different groups divided by age (**B**), stage (**C**) and LN-metastasis (**D**). **E, F** CCK-8 assay was used to evaluate the proliferation effect of SLC3A2. **G** Effect of SLC3A2 on invasion assessed using the Transwell assay

Discussion

The occurrence of EC has been on a rising trend, making it the most prevalent gynecological tumor in developed countries and some advanced urban areas in developing countries [22–24]. Contributing factors to this increase include the prevalence of chronic conditions such as obesity, diabetes, and hypertension, with the incidence of EC growing annually by 1.9% [25, 26]. Fortunately, many EC patients exhibit early symptoms like abnormal vaginal bleeding, allowing for early diagnosis and effective treatment. However, in cases where early symptoms of EC are subtle or overlooked, and the disease progresses to advanced stages of metastasis and invasion, the 5-year survival rate drops to a concerning 16–45% [27]. This stark contrast in outcomes based on the stage of

diagnosis underscores the urgency in identifying effective therapeutic targets, and prognostic markers and predicting chemotherapy drug sensitivity for EC. Such advancements are crucial for enhancing patient survival rates and improving the overall management of this increasingly common disease.

Regulating cell death is (RCD) an important way for the body to combat the malignant proliferation of tumor cells. Like other RCDs, the elucidation of disulfidptosis will provide new ideas for understanding and targeting cancer therapies [28]. Although disulfidptosis has only been a newly identified RCD for a short time, there is growing evidence that disulfidptosis plays an important role in tumors [29, 30]. Previous studies have shown that the disulfidptosis related gene SLC7A11 influences the

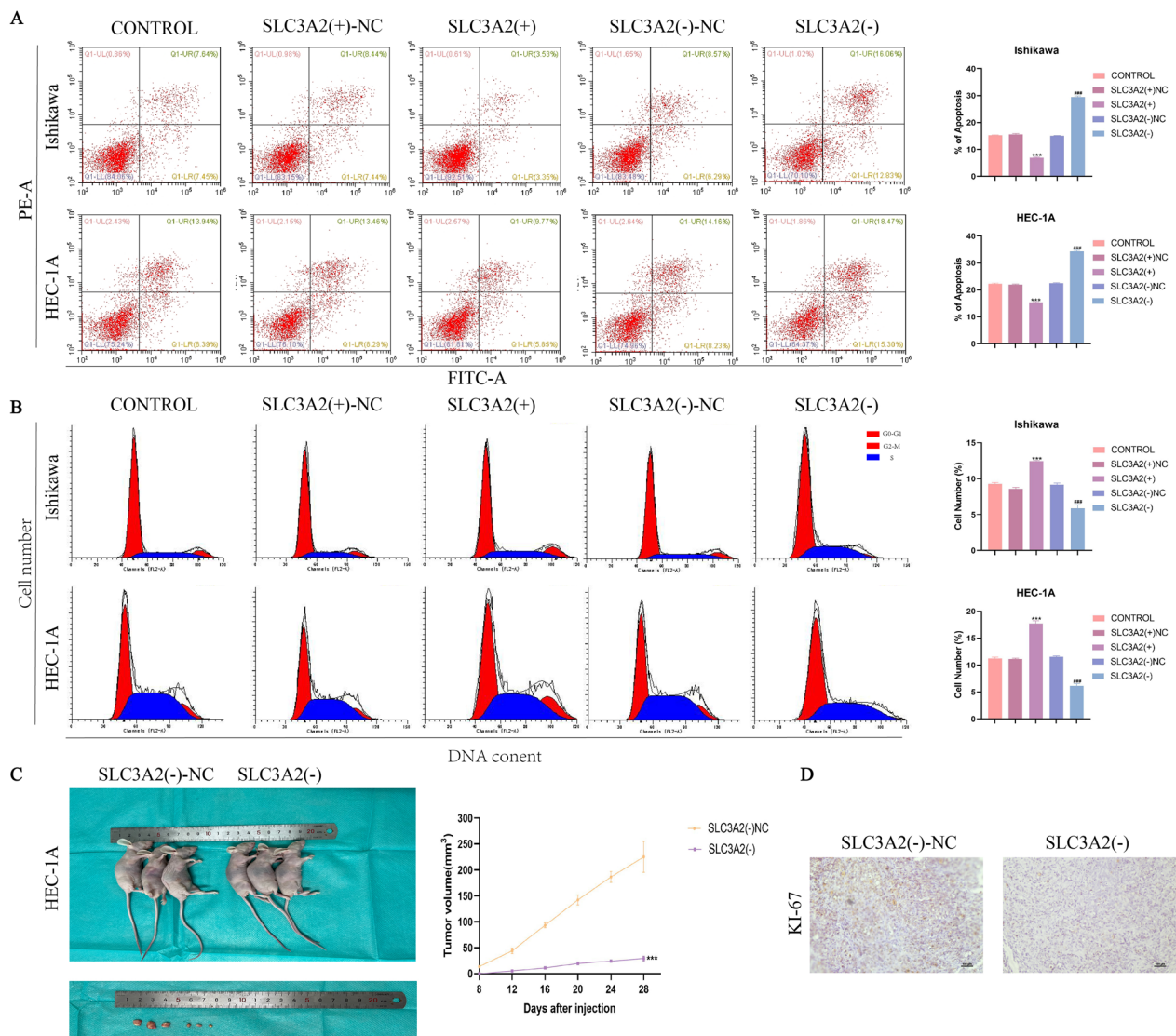


Fig. 8 SLC3A2 regulates the biological behavior of EC cell lines and In vivo study of tumor xenografts. **A** Cell apoptosis assay was used to determine the effect of SLC3A2 on the apoptosis of Ishikawa and HEC-1A cell lines. **B** Cell cycle analysis was used to detect the effect of SLC3A2 on the cell cycle of Ishikawa and HEC-1A cell lines. **C** The nude mice carrying tumors from the respective groups are shown. The sample tumors from the respective groups are shown (n=3, each group). **D** Expression levels of Ki-67

sensitivity of cancer cells to oxidative stress [31]. In addition, existing studies have shown that DRGs is associated with the prognosis of liver, lung, and colorectal cancers [32–35]. However, DGRs has not been reported in EC. Therefore, we hope to establish a DRGs-based model to predict EC prognosis and find EC therapeutic targets.

We performed univariate analysis of 24 DRGs and found that 7 DRGs were associated with OS. We then constructed a prognostic model of EC by Lasso-Cox regression analysis. We further constructed a nomogram to optimize the model. Meanwhile, comparative analysis shows that our model performs better than existing

models. The results of correlation analysis showed that the higher pathological parameters group (stage III–IV, grade 3–4, and age >65.) had a higher risk score, indicating that the risk score was positively correlated with clinical risk factors. Immunotype analysis showed the highest risk score in C2, which had the worst prognosis [36]. These results all support a poorer prognosis in the high-risk group.

Prior research has established a connection between disulfidptosis-related genes and the tumor microenvironment [37, 38]. Consistent with these findings, our study also reveals a significant relationship between

disulfidptosis-related genes (DRGs) and the immune microenvironment in tumors. Through correlation analysis, we observed a suppression of immune cells and their functions in patients categorized in the high-risk group. Notably, the proportions of immune dendritic cells (iDCs), neutrophils, T helper cells, and tumor-infiltrating lymphocytes (TIL) were substantially reduced in this group. These findings suggest that DRGs may play a pivotal role in tumor progression and patient prognosis, potentially by impeding cellular immune functions. This insight opens up new avenues for understanding the mechanisms of tumor immune evasion and highlights the potential of DRGs as targets for therapeutic intervention. By modulating these genes, there may be opportunities to enhance immune response and improve patient outcomes in EC.

The correlation analysis conducted in our study between the risk score and the tumor immune microenvironment revealed a significant positive relationship between the risk score and RNA stemness score (RNAss), which is indicative of cancer stem cell (CSC) levels. CSCs are characterized by their self-renewal capacity and are known to contribute to resistance against immunotherapy and chemotherapy. This insight is crucial as it underlines the role of CSCs in the persistence and treatment resistance of tumors [39, 40]. Overall, our findings suggest that dysregulation of DRGs may lead to abnormalities in disulfidptosis, a process that could potentially exacerbate the aggressiveness of endometrial cancer. This dysregulation could enhance the stemness properties of cancer cells, thereby contributing to the resilience of the tumor against conventional therapies. Understanding these mechanisms is helpful in the treatment of EC.

Chemotherapy and immunotherapy play an important role in the treatment of EC as an important supplement to surgical treatment of EC [41, 42]. However, there are still few studies on EC predicting immunotherapy and chemotherapy sensitivity [43]. In our study, there was no significant difference in risk scores between patients on immunotherapy PD or SD and patients on immunotherapy PR or CR. In our study, the high-risk group was more sensitive to cisplatin, dasatinib, doxorubicin, and paclitaxel compared to the low-risk group. cisplatin and doxorubicin are first-line chemotherapeutic agents for EC treatment [44, 45]. Therefore, our model predicts that high-risk groups can be treated with chemotherapy drugs rather than expensive immunotherapy. These predictions could not only lead to better treatment of EC patients, but also reduce the medical burden.

To further screen key genes in the model, we used random forest methods to screen 24 DRGs. Finally, we identified the key gene SLC3A2 in the model. Expression analysis showed that SLC3A2 expression was elevated

in EC. In order to further verify the key role of SLC3A2 in endometrial cancer, we conducted experimental verification. In this study, we verified the ability of SLC3A2 to promote tumor growth and metastasis through both in vitro and in vivo experiments. Existing studies have shown that the high expression of SLC3A2 in most tumors, including lung cancer and ovarian cancer, is associated with prognosis and promotion of tumor progression [46, 47].

Our research was constrained by the absence of external datasets containing clinical data relevant to UCEC, other than the UCEC-TCGA dataset. Consequently, we were only able to perform internal validation using the UCEC-TCGA data. This limitation signifies that the findings and conclusions drawn from our study are primarily based on the analysis of the UCEC-TCGA dataset and might not be fully generalizable to broader populations or other datasets. Future research would benefit from incorporating external datasets for validation, which would strengthen the reliability and applicability of the prognostic model and findings to a wider array of clinical scenarios. meantime, our model has not been applied in clinical practice, and we will further apply it in clinical practice in the future. In addition, the DRGs model obtained based on the TCGA database needs more experiments to prove the specific molecular mechanism by correlation analysis with the immune microenvironment, tumor stem cells and GSEA.

Nevertheless, we have for the first time relied on DRGs to construct a prognostic model and accurately predict the prognosis of patients. Furthermore, we also identified SLC3A2, a key gene in the prognostic model of DRGs, and demonstrated that SLC3A2 is promising as a diagnostic, prognostic indicator and therapeutic target.

Conclusion

The development of our new DRGs-based model has some significance in predicting the prognosis of EC patients. We found that SLC3A2 is a key gene in this model. SLC3A2 is expected to be a diagnostic, prognostic and therapeutic target. These findings have important clinical implications and provide potential value for enhanced treatment.

Abbreviations

EC	Endometrial cancer
UCEC	Uterine corpus endometrial cancer
DRGs	Disulfidptosis-related genes
DEDRGs	Differentially expressed disulfidptosis-related genes
TCGA	The Cancer Genome Atlas
TME	The tumor microenvironment
CSCs	Cancer stem cells
LASSO	Least absolute shrinkage and selection operator
KM	Kaplan–Meier
ROC	Receiver operating characteristic
AUCs	Areas under the ROC curves

ssGSEA	Single-sample gene set enrichment analysis
RNAss	RNA stemness scores
DNAss	DNA stemness scores
qRT-PCR	Quantitative real-time PCR
mRNA	Messenger RNA
OS	Overall survival
GO	Gene ontology
KEGG	Kyoto encyclopedia of genes and genomes
SLC3A2	Solute carrier family 3 member 2

Supplementary Information

The online version contains supplementary material available at <https://doi.org/10.1186/s12935-024-03560-6>.

Supplementary material 1.

Supplementary material 2: Figure S1 Construction of prognosis model (A) Survival curves and (B) ROC curves of high and low risk groups in the training group. (C) The risk score value of each sample, (D) the survival status ranked from low to high-risk scores in the training group. (E) Survival curves and (F) ROC curves of high and low risk groups in the test group. (G) The risk score value of each sample, (H) the survival status ranked from low to high-risk scores in the test group. (I–J) Univariate and multivariate analysis were performed to assess the clinicopathological prognostic value of the prediction model. (K) ROC curves for predicting the 1-, 3-, and 5-year OS of UCEC patients. (L) Decision Curve Analysis (DCA) curves for predicting the 1-, 3-, and 5-year OS of UCEC patients.

Acknowledgements

The authors thank members of their laboratory and collaborators for supporting this research.

Author contributions

BW, FK and XM designed the study. BW and XW performed the experiments mentioned in the paper. YW drafted the manuscript. ZW, WW and HL were involved in collating the data. All authors participated in manuscript editing. All authors read and approved the final manuscript.

Funding

Our study was supported by the China Medical University's 2018 Discipline Construction "Major Special Construction Plan" (No. 3110118029), and Outstanding Scientific Fund of Shengjing Hospital (No. 201601).

Availability of data and materials

No datasets were generated or analysed during the current study.

Declarations

Ethics approval and consent to participate

This study was approved by the Institutional Review Committee (Ethical No. 2018PS251K, 2018PS136K) of the Shengjing Hospital affiliated to China Medical University, and experimentation was conducted based on the approved guidelines.

Consent for publication

We have obtained consent to publish this paper from all the participants of this study.

Competing interests

The authors declare no competing interests.

Received: 3 January 2024 Accepted: 4 November 2024
Published online: 28 November 2024

References

- Bray F, Ferlay J, Soerjomataram I, Siegel RL, Torre LA, Jemal A. Global cancer statistics 2018: GLOBOCAN estimates of incidence and mortality worldwide for 36 cancers in 185 countries. *CA Cancer J Clin*. 2018;68(6):394–424.
- Crosbie EJ, Kitson SJ, McAlpine JN, Mukhopadhyay A, Powell ME, Singh N. Endometrial cancer. *Lancet*. 2022;399(10333):1412–28.
- Nagy P. Kinetics and mechanisms of thiol-disulfide exchange covering direct substitution and thiol oxidation-mediated pathways. *Antioxid Redox Signal*. 2013;18(13):1623–41.
- Trivedi MV, Laurence JS, Siahaan TJ. The role of thiols and disulfides on protein stability. *Curr Protein Pept Sci*. 2009;10(6):614–25.
- Liu X, Nie L, Zhang Y, Yan Y, Wang C, Colic M, Olszewski K, Horbath A, Chen X, Lei G, et al. Actin cytoskeleton vulnerability to disulfide stress mediates disulfidptosis. *Nat Cell Biol*. 2023;25(3):404–14.
- Nagy P. Kinetics and mechanisms of thiol-disulfide exchange covering direct substitution and thiol oxidation-mediated pathways. *Antioxid Redox Signal*. 2013;18(13):1623–41.
- Zheng P, Zhou C, Ding Y, Duan S. Disulfidptosis: a new target for metabolic cancer therapy. *J Exp Clin Cancer Res*. 2023;42(1):103.
- Zhong Z, Zhang C, Ni S, Ma M, Zhang X, Sang W, Lv T, Qian Z, Yi C, Yu B. NFATc1-mediated expression of SLC7A11 drives sensitivity to TXNRP1 inhibitors in osteoclast precursors. *Redox Biol*. 2023;63:102711.
- Wang T, Guo K, Zhang D, Wang H, Yin J, Cui H, Wu W. Disulfidptosis classification of hepatocellular carcinoma reveals correlation with clinical prognosis and immune profile. *Int Immunopharmacol*. 2023;120:110368.
- Qi C, Ma J, Sun J, Wu X, Ding J. The role of molecular subtypes and immune infiltration characteristics based on disulfidptosis-associated genes in lung adenocarcinoma. *Aging (Albany NY)*. 2023;15(11):5075–95.
- Chen H, Yang W, Li Y, Ma L, Ji Z. Leveraging a disulfidptosis-based signature to improve the survival and drug sensitivity of bladder cancer patients. *Front Immunol*. 2023;14:1198878.
- Shin CS, Mishra P, Watrous JD, Carelli V, D'Aurelio M, Jain M, Chan DC. The glutamate/cystine xCT antiporter antagonizes glutamine metabolism and reduces nutrient flexibility. *Nat Commun*. 2017;8:15074.
- Koppula P, Zhang Y, Shi J, Li W, Gan B. The glutamate/cystine antiporter SLC7A11/xCT enhances cancer cell dependency on glucose by exporting glutamate. *J Biol Chem*. 2017;292(34):14240–9.
- Goji T, Takahara K, Negishi M, Katoh H. Cystine uptake through the cystine/glutamate antiporter xCT triggers glioblastoma cell death under glucose deprivation. *J Biol Chem*. 2017;292(48):19721–32.
- Liu X, Olszewski K, Zhang Y, Lim EW, Shi J, Zhang X, Zhang J, Lee H, Koppula P, Lei G, et al. Cystine transporter regulation of pentose phosphate pathway dependency and disulfide stress exposes a targetable metabolic vulnerability in cancer. *Nat Cell Biol*. 2020;22(4):476–86.
- Simon N, Friedman J, Hastie T, Tibshirani R. Regularization paths for Cox's proportional hazards model via coordinate descent. *J Stat Softw*. 2011;39(5):1–13.
- Yoshihara K, Shahmoradgoli M, Martínez E, Vegesna R, Kim H, Torres-García W, Treviño V, Shen H, Laird PW, Levine DA, et al. Inferring tumour purity and stromal and immune cell admixture from expression data. *Nat Commun*. 2013;4:2612.
- Malta TM, Sokolov A, Gentles AJ, Burzykowski T, Poisson L, Weinstein JN, Kamińska B, Huelken J, Omberg L, Gevaert O, et al. Machine learning identifies stemness features associated with oncogenic dedifferentiation. *Cell*. 2018;173(2):338–354.e315.
- Cai L, Hu C, Yu S, Liu L, Zhao J, Zhao Y, Lin F, Du X, Yu Q, Xiao Q. Identification of EMT-related gene signatures to predict the prognosis of patients with endometrial cancer. *Front Genet*. 2020;11:582274.
- Liu J, Li S, Feng G, Meng H, Nie S, Sun R, Yang J, Cheng W. Nine glycolysis-related gene signature predicting the survival of patients with endometrial adenocarcinoma. *Cancer Cell Int*. 2020;20:183.
- Liu J, Mei J, Li S, Wu Z, Zhang Y. Establishment of a novel cell cycle-related prognostic signature predicting prognosis in patients with endometrial cancer. *Cancer Cell Int*. 2020;20:329.
- Siegel RL, Miller KD, Jemal A. Cancer statistics, 2017. *CA Cancer J Clin*. 2017;67(1):7–30.
- Siegel RL, Miller KD, Jemal A. Cancer statistics, 2018. *CA Cancer J Clin*. 2018;68(1):7–30.
- Siegel RL, Miller KD, Jemal A. Cancer statistics, 2020. *CA Cancer J Clin*. 2020;70(1):7–30.

25. Lauby-Secretan B, Scoccianti C, Loomis D, Grosse Y, Bianchini F, Straif K. Body fatness and cancer—viewpoint of the IARC working group. *N Engl J Med*. 2016;375(8):794–8.
26. Rahib L, Smith BD, Aizenberg R, Rosenzweig AB, Fleshman JM, Matrisian LM. Projecting cancer incidence and deaths to 2030: the unexpected burden of thyroid, liver, and pancreas cancers in the United States. *Cancer Res*. 2014;74(11):2913–21.
27. Weiderpass E, Antoine J, Bray FI, Oh JK, Arbyn M. Trends in corpus uteri cancer mortality in member states of the European Union. *Eur J Cancer*. 2014;50(9):1675–84.
28. Zhao D, Meng Y, Dian Y, Zhou Q, Sun Y, Le J, Zeng F, Chen X, He Y, Deng G. Molecular landmarks of tumor disulfidptosis across cancer types to promote disulfidptosis-target therapy. *Redox Biol*. 2023;68:102966.
29. Liu X, Zhuang L, Gan B. Disulfidptosis: disulfide stress-induced cell death. *Trends Cell Biol*. 2023. <https://doi.org/10.1016/j.tcb.2023.07.009>.
30. Hadian K, Stockwell BR. The therapeutic potential of targeting regulated non-apoptotic cell death. *Nat Rev Drug Discov*. 2023;22(9):723–42.
31. Yan Y, Teng H, Hang Q, Kondiparthi L, Lei G, Horbath A, Liu X, Mao C, Wu S, Zhuang L, et al. SLC7A11 expression level dictates differential responses to oxidative stress in cancer cells. *Nat Commun*. 2023;14(1):3673.
32. Wang Z, Chen X, Zhang J, Chen X, Peng J, Huang W. Based on disulfidptosis-related glycolytic genes to construct a signature for predicting prognosis and immune infiltration analysis of hepatocellular carcinoma. *Front Immunol*. 2023;14:1204338.
33. Xue W, Qiu K, Dong B, Guo D, Fu J, Zhu C, Niu Z. Disulfidptosis-associated long non-coding RNA signature predicts the prognosis, tumor micro-environment, and immunotherapy and chemotherapy options in colon adenocarcinoma. *Cancer Cell Int*. 2023;23(1):218.
34. Wang Y, Xu Y, Liu C, Yuan C, Zhang Y. Identification of disulfidptosis-related subgroups and prognostic signatures in lung adenocarcinoma using machine learning and experimental validation. *Front Immunol*. 2023;14:1233260.
35. Zhang HB, Pan JY, Zhu T. A disulfidptosis-related lncRNA prognostic model to predict survival and response to immunotherapy in lung adenocarcinoma. *Front Pharmacol*. 2023;14:1254119.
36. Thorsson V, Gibbs DL, Brown SD, Wolf D, Bortone DS, Ou Yang TH, Porta-Pardo E, Gao GF, Plaisier CL, Eddy JA, et al. The Immune Landscape of Cancer. *Immunity*. 2018;48(4):812–830.e814.
37. Liang J, Wang X, Yang J, Sun P, Sun J, Cheng S, Liu J, Ren Z, Ren M. Identification of disulfidptosis-related subtypes, characterization of tumor microenvironment infiltration, and development of a prognosis model in breast cancer. *Front Immunol*. 2023;14:1198826.
38. Liao Z, Cheng Y, Zhang H, Jin X, Sun H, Wang Y, Yan J. A novel prognostic signature and immune microenvironment characteristics associated with disulfidptosis in papillary thyroid carcinoma based on single-cell RNA sequencing. *Front Cell Dev Biol*. 2023;11:1308352.
39. Visvader JE, Lindeman GJ. Cancer stem cells: current status and evolving complexities. *Cell Stem Cell*. 2012;10(6):717–28.
40. Atashzar MR, Baharlou R, Karami J, Abdollahi H, Rezaei R, Pourramezan F, Zoljalali Moghaddam SH. Cancer stem cells: a review from origin to therapeutic implications. *J Cell Physiol*. 2020;235(2):790–803.
41. Fillon M. Adding immunotherapy to chemotherapy improves survival for endometrial cancer patients. *CA Cancer J Clin*. 2023;73(5):445–7.
42. Polak P, Fu L, Foulkes WD. PD-1 and PD-L1 blockade plus chemotherapy in endometrial cancer. *N Engl J Med*. 2023;389(9):866.
43. Rochigneux P, Garcia AJ, Chanez B, Madroszyk A, Olive D, Garon EB. Medical treatment of lung cancer: can immune cells predict the response? A systematic review. *Front Immunol*. 2020;11:1036.
44. Susumu N, Sagae S, Udagawa Y, Niwa K, Kuramoto H, Satoh S, Kudo R. Randomized phase III trial of pelvic radiotherapy versus cisplatin-based combined chemotherapy in patients with intermediate- and high-risk endometrial cancer: a Japanese Gynecologic Oncology Group study. *Gynecol Oncol*. 2008;108(1):226–33.
45. Randall ME, Filiaci VL, Muss H, Spirto NM, Mannel RS, Fowler J, Thigpen JT, Benda JA. Randomized phase III trial of whole-abdominal irradiation versus doxorubicin and cisplatin chemotherapy in advanced endometrial carcinoma: a Gynecologic Oncology Group Study. *J Clin Oncol*. 2006;24(1):36–44.
46. El Ansari R, Craze ML, Diez-Rodriguez M, Nolan CC, Ellis IO, Rakha EA, Green AR. The multifunctional solute carrier 3A2 (SLC3A2) confers a poor prognosis in the highly proliferative breast cancer subtypes. *Br J Cancer*. 2018;118(8):1115–22.
47. Liu D, An M, Wen G, Xing Y, Xia P. Both in situ and circulating SLC3A2 could be used as prognostic markers for human lung squamous cell carcinoma and lung adenocarcinoma. *Cancers*. 2022;14(21):5191.

Publisher's Note

Springer Nature remains neutral with regard to jurisdictional claims in published maps and institutional affiliations.